

Mechanism and Stereoselectivity of Directed C(sp³)-H Activation and Arylation Catalyzed by Pd(II) with Pyridine Ligand and Trifluoroacetate: A Computational Study

Julong Jiang,[†] Jin-Quan Yu,[‡] and Keiji Morokuma^{*,†}

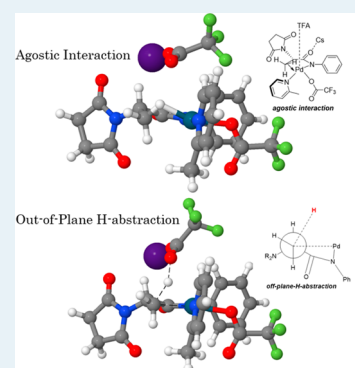
[†]Fukui Institute for Fundamental Chemistry, Kyoto University, Kyoto 606-8103, Japan

[‡]Department of Chemistry, The Scripps Research Institute, 10550 North Torrey Pines Road, La Jolla, California 92037, United States

Supporting Information

ABSTRACT: Density functional theory (DFT) calculations were conducted to elucidate the mechanism of a novel Pd(II) catalyzed C(sp³)-H activation and the subsequent arylation reactions of amides in the presence of pyridine derivatives as ligands. All plausible pathways were carefully studied, and the minimum energy pathway was located successfully. Being different from most of the C-H activation reactions, 2-picoline used in this reaction reacts with Pd(TFA)₂ (trifluoroacetate) to form a very stable precatalyst. Measures should thus be taken to activate the precatalyst, including the modification of the amide substrate and a proper choice of solvent. Our calculations helped to reveal the relevant details. An unconventional deprotonation mechanism for the C-H activation step, which is different from the traditional CMD (or AMLA) mechanism, was found through our theoretical studies. The methyl group is deprotonated by an *out-of-plane* (external) TFA, rather than a TFA ligand directly bound to the Pd(II) atom. As part of the uncommon Pd(II)-Pd(IV)-Pd(II) catalytic cycle, the succeeding arylation reaction, which takes place on the product of the C-H activation reaction, was also studied by us. The arylation reaction was found to have a lower barrier compared to that of the C-H activation reaction, which confirms that the C-H activation is the rate-determining step. On the basis of our newly found minimum energy pathway (MEP), the secondary C(sp³)-H activation reaction was also investigated and the results helped us to unveil the origins of the diastereoselectivity. Some other aspects that affect the C-H activation, such as the agostic interaction and the ligand effect, were also discussed in this article.

KEYWORDS: C(sp³)-H activation, C(sp²)-H activation, unconventional CMD (or AMLA), *out-of-plane* H-abstraction, agostic interaction, diastereoselectivity



INTRODUCTION

One of the most important applications of homogeneous catalyst is to catalyze those reactions which are employed to synthesize bioactive compounds. Among those reactions, the transition-metal catalyzed C-C cross-coupling reaction is the most popular approach, since it offers a straightforward way to construct the carbon framework of those useful precursors in pharmaceutical industry. During the past several decades, efforts have been made for the exploration of the transition-metal catalyzed cross-coupling reactions.¹ Some of them have already been used as a general way to construct C-C bonds.²⁻⁶ However, in most cases, a specific substrate should be synthesized prior to the subsequent cross-coupling reaction. It should be noted that these special substrates are not always easy to prepare and sometimes suffer from decomposition due to the instability.⁷

In recent years, more attention has been alternatively directed to direct C-H activation. Direct C-H activation has the potential to become a general strategy to construct and functionalize organic molecules in the future. However, due to the high stability and strength of the C-H bond, it is not trivial to find a proper catalyst to achieve the goal. Nevertheless, some

achievements have been made on the Pd-catalyzed C-H activation reactions, mainly for the C(sp²)-H bond of arenes.⁸⁻¹⁰ Recently, the Yu group reported a novel C(sp³)-H activation and the subsequent arylation reaction of alanine derivatives, which is catalyzed by a Pd(II) catalyst (Scheme 1).¹¹ The ligands are as simple as pyridine derivatives. A careful choice of the ligands makes the subsequent secondary C(sp³)-H bond arylation reaction feasible in a stereoselective manner.

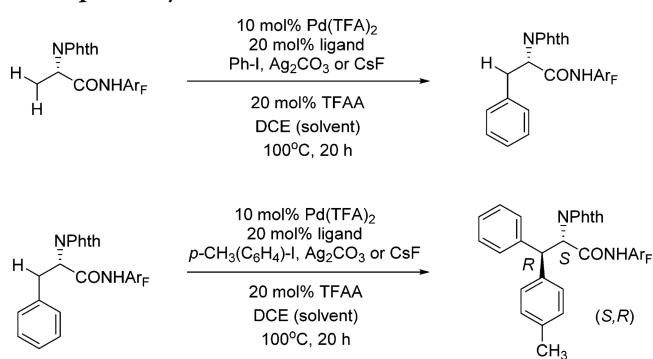
More interestingly, as shown in Scheme 2, the intermediates A and B generated through C-H activation have been successfully isolated and characterized. 2-Methylpyridine (2-picoline) was found as an appropriate ligand for the primary C(sp³)-H activation, whereas an electron-rich ligand (2-alkoxyquinoline) was used for the secondary C(sp³)-H bond. The reaction conditions become much milder with the help of 2-alkoxyquinoline.

Different from most of the C-H activation reactions developed before, an extra ligand (2-picoline) present in this

Received: October 21, 2014

Revised: April 27, 2015

Published: May 1, 2015

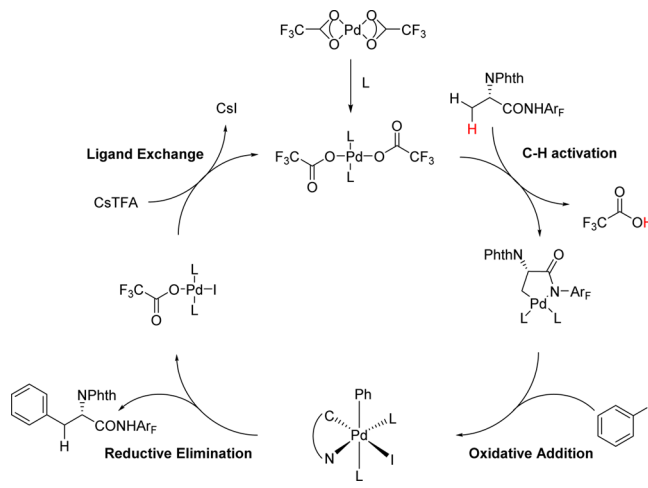
Scheme 1. Palladium-Catalyzed C(sp³)-H Activation and Subsequent Arylation¹¹

reaction can react with Pd(TFA)₂ (trifluoroacetate) to form a stable precatalyst. How to activate the inert precatalyst is what we are trying to understand. To allow a C–H activation reaction, vacancies should be generated at the Pd(II) center. Moreover, the palladium employed in this reaction undergoes an uncommon Pd(II)–Pd(IV)–Pd(II) catalytic cycle. Our work aims at providing a detailed mechanism of this one-pot reaction, so that the application of this reaction may be extended. For the convenience of discussion of reaction steps, we therefore give a generic mechanism for this catalytic reaction shown in Scheme 3, consisting of a C–H activation followed by the oxidative addition and reductive elimination reactions.

In the present theoretical study of this one-pot reaction, the focus was mainly put on the C(sp³)-H activation step. Density functional theory (DFT) calculations helped us to understand the details of the C–H activation, including how to activate the precatalyst, the exact way for the base to deprotonate the methyl group and the origins of the diastereoselectivity. Some other aspects, like factors that promote the C–H activation step, were also discussed in this article. Suggestions to the experimentalists were provided accordingly, based on our theoretical findings.

■ COMPUTATIONAL DETAILS

All of the calculations were carried out at DFT level of theory with B3LYP hybrid functional.^{12,13} The B3LYP functional was corrected with the empirical dispersion term (known as Grimme-D3¹⁴), as implemented in Gaussian09.¹⁵ The 6-311G(d,p) basis set¹⁶ was employed for C, H, O, N, and F atoms. The SDD basis set,¹⁷ an effective core potential basis set, was used for I and Pd atoms with additional d- and f-

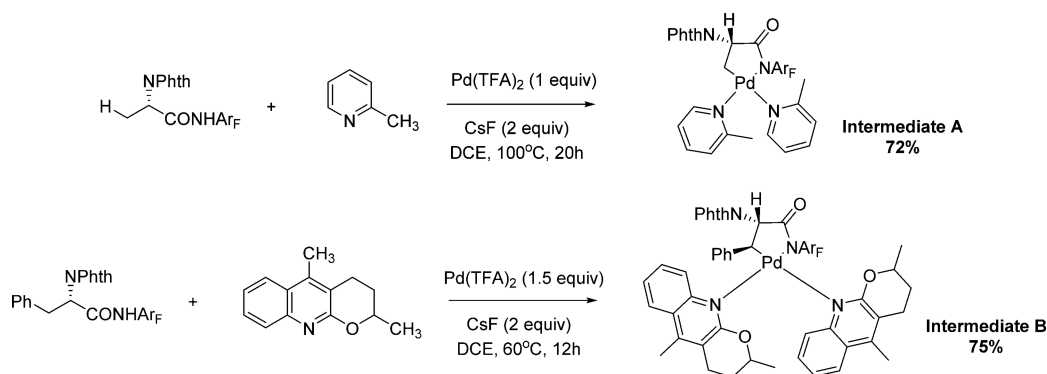
Scheme 3. Generic Mechanism of the Entire Catalytic Cycle

polarization function ($\zeta_d = 0.289$, $\zeta_f = 1.472$),^{18,19} respectively. The transition states were located by means of the QST3 method^{20,21} and the Berny algorithm.²² All of the reactant, intermediate, transition state, and product structures were fully optimized without any symmetric restrictions. Solvent effect was introduced through IEF-PCM model^{23–26} as implemented in Gaussian09 with dichloroethane as the solvent ($\epsilon = 10.125$).

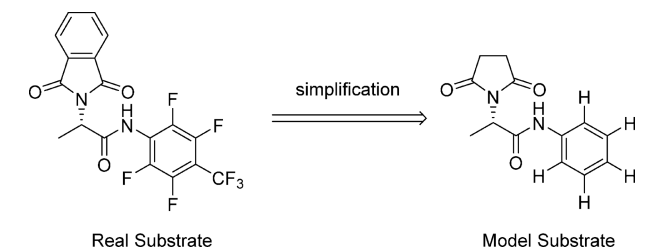
Frequency calculations were conducted to ensure the structure obtained is a minimum or a transition state. Intrinsic reaction coordinate (IRC) calculation²⁷ was conducted to confirm that the transition state is connected to the correct reactant and product. All of the enthalpies and Gibbs energies shown in this article were calculated at 1 atm and 298.15 K. The atomic partial charges were calculated following the population analysis based on the atomic polarization tensor.²⁸

In order to thoroughly explore many possible reaction pathways without too heavy computational cost, a model substrate, **Sub_Ph**, was employed in our study. All fluorine atoms on the benzene ring of the real substrate are replaced by hydrogen atoms, as shown in Scheme 4. The 2-picoline ligand is fully considered without any simplification. Nevertheless, calculations with the real substrate were also conducted for the minimum energy pathway (MEP) to ensure there is no significant difference with respect to the simplification, which will be demonstrated in later sections.

How to handle the entropy contribution in solution has been raised as a question for a long time.^{29–32} The translational and rotational motions of molecules in solution are restrained due

Scheme 2. Generation of Intermediate A and Intermediate B¹¹

Scheme 4. Model Substrate, Sub_Ph, Used in the Calculation



to solvent effects, which is different from the situation in the gas phase. The PCM model fails to give a good description of the situation where the solute molecules stay in. It has been noticed, if the number of molecules changes during the reaction, the entropy contribution to the reaction Gibbs energy change is largely overestimated with the PCM solvation model.^{33,34} A very recent article from the Singleton group carefully evaluated the entropy problem by conducting a comprehensive study of both experimental data and calculations results.³⁵ For association and dissociation reactions, a full inclusion of the calculated entropy would lead to the wrong conclusion, as suggested in the above article. From a simple model for the solvation of methanol in cyclohexanone, as shown in Scheme S10 in the Supporting Information (SI), we found that the change of enthalpy is very close to the experimental data,³⁶ whereas the Gibbs energy change for the solvation is far from accurate. Therefore, enthalpies and Gibbs energies are systematically shown in all figures. If the number of molecules changes during the reaction, like what can be observed in ligand dissociation and association reactions, enthalpy is preferred over Gibbs energy to describe the change of energy.

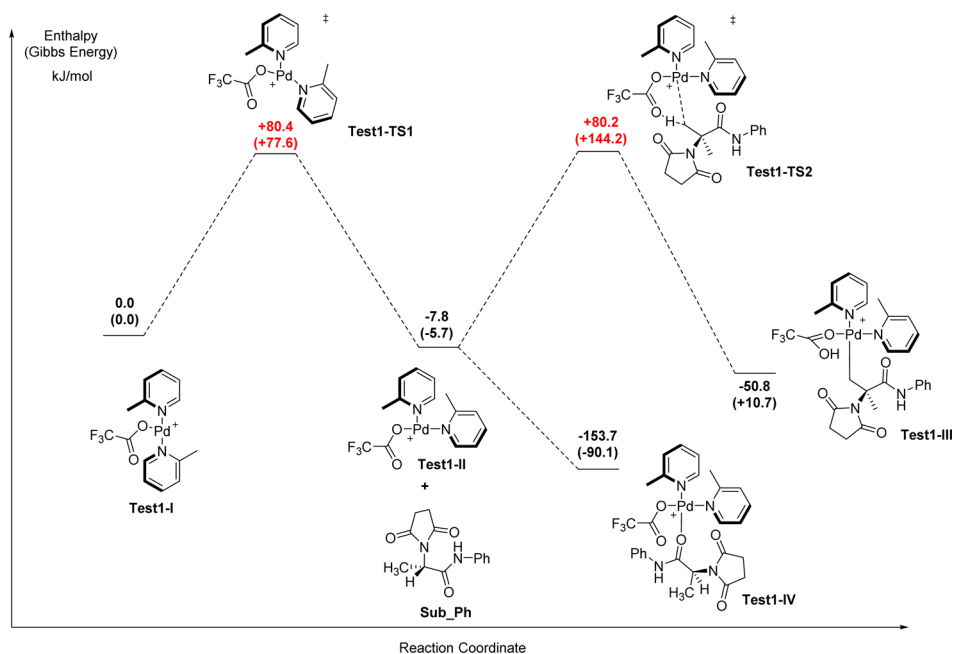
RESULTS AND DISCUSSIONS

1. Initiation of the C–H Activation Step. 1.1. High Stability of the Four-Coordinate Pd(II) Complex. Although we know the fact that Pd(II) intends to adopt a four-coordinate square planar geometry, the energy penalty for distorting such a stable geometry was not studied quantitatively. To allow a C–H activation reaction, a vacant-site at the Pd(II) center should be created for the newly formed Pd–C bond. Thus, our initial test calculations were focused on the pathways involving direct interactions between a three-coordinate Pd(II) catalyst and the amide substrate. Among them, two pathways which have the lowest effective barriers are shown below in Scheme 5 and Scheme S1 (in the SI).

In Scheme 5, the reaction starts with the cationic complex **Test1-I**, which is a three-coordinate Pd(II) complex. Since the TFA ligand is responsible for the deprotonation, the first step in this pathway is the rearrangement of the ligands to create a vacancy cis to the TFA. The rearrangement results in the formation of **Test1-II** in which two 2-picoline ligands are cis to each other. The larger stability of the intermediate **Test1-II** by 7.8 kJ/mol over **Test1-I** is likely to be caused by the electronic effect that 2-picoline ligand has a stronger trans influence than TFA. The enthalpy barrier for the ligand rearrangement at **Test1-TS1** is 80.4 kJ/mol (77.8 kJ/mol for the Gibbs barrier).

The transition state for the deprotonation, **Test1-TS2**, has a relative enthalpy of +80.2 kJ/mol with respect to that of **Test1-I**. However, further investigation revealed an extremely stable four-coordinate intermediate **Test1-IV** generated by the coordination of the carbonyl group of **Sub_Ph** to the Pd(II) center. Thus, the pathway shown in Scheme 5 is not the correct reaction mechanism, given that the effective enthalpy barrier is as high as 233.9 kJ/mol.

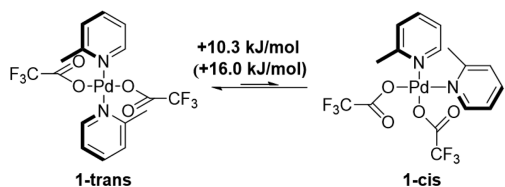
The same thing happens if starting with **Test2-I**, a three-coordinate neutral complex Pd(II)(TFA)₂(2MP). As shown in Scheme S1 in the SI, the C–H activation is blocked, given the fact that the four-coordinate Pd(II) intermediate **Test2-III** is

Scheme 5. Enthalpy Profile for the C–H Activation Starting with Cationic Three-Coordinate Pd(II) Complex (**Test1-I**) in DCE (Gibbs Energy Shown in Parentheses)

very stable so that the effective barrier of the C–H activation is 233.9 kJ/mol.

From the quantitative analysis of the reaction pathways shown above, we recognized that any distortion from the square planar geometry will cost an unaffordable energetic penalty. Extra calculations at this stage indicated that the coordination of 2-picoline to the Pd(II) atom is highly favorable (see Scheme S9 in the SI for more details). Although trifluoroacetate anion can play the role as a bidentate ligand in the monomer of Pd(TFA)₂, one of the Pd–O bonds is extremely weak compared to the Pd–N bond. Breaking one of the Pd–O bonds by adding a 2-picoline ligand gives a huge stabilization enthalpy of –175.5 kJ/mol. As shown in Scheme 6,

Scheme 6. Equilibrium between the Precatalysts 1-trans and 1-cis (Gibbs Energy Shown in Parentheses)



1-trans is more stable than **1-cis** by 16.0 kJ/mol (10.0 kJ/mol for the enthalpy difference). Moreover, the barrier for intramolecular conversion between these two isomers is extremely high, which is similar to the case of *trans*-platinum and the cisplatin.

Our computational results are also supported by the experimental data which was reported by Stoltz et al.³⁷ The four-coordinate Pd(II) complex **1-trans** can be synthesized in a standard procedure. Based on our calculation results, the reaction pathways starting with **1-trans** as the precatalyst are more favorable. Further calculations also showed that the neutral amide substrate (**Sub_Ph**) is not nucleophilic enough to substitute TFA or 2-picoline ligand in **1-trans** as shown in Scheme S3 in the SI. Based on the results demonstrated above,

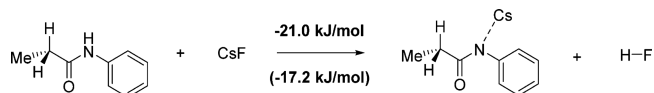
at least two vacancies are required for the C–H activation. One is for the amide substrate to fix to the Pd(II) center and the other one is reserved for the C–Pd bond.

1.2. Selection Criteria of the Amide Substrate. As a conclusion from the previous studies demonstrated in section 1.1, the precatalyst (**1-trans** and **1-cis**) for the C–H activation is very stable and even inert. Efforts are needed to understand how this inert precatalyst gets activated. Inspired by the work done by Musaev and co-workers,³⁸ the structure of amides was the first thing to investigate.

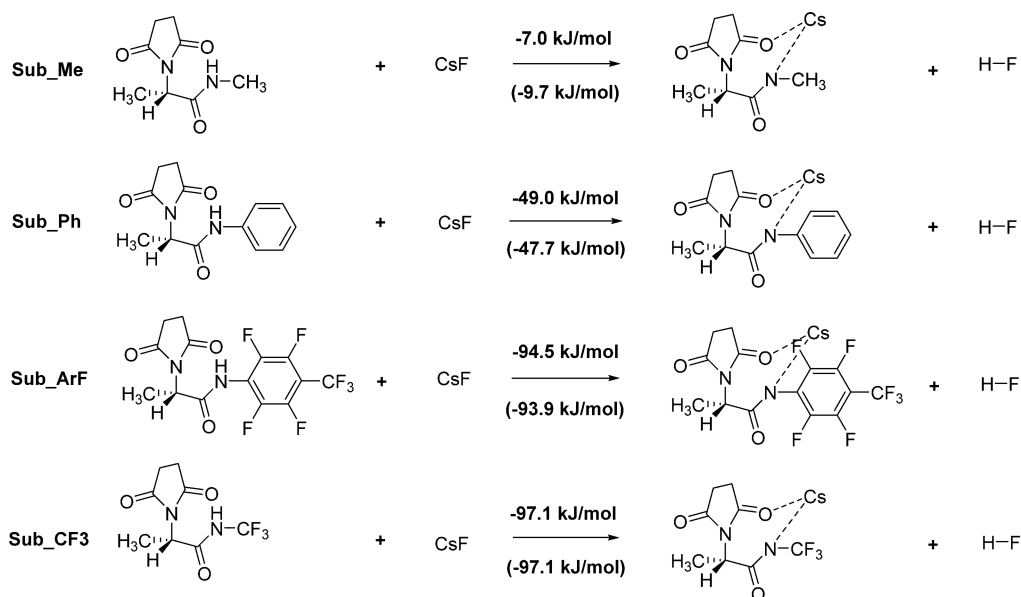
As shown in Scheme 7, the effect of the functional groups on the deprotonation has been studied quantitatively. It was not surprising that an aromatic ring promotes the deprotonation due to the delocalization effect. However, our results gave a clearer picture for the selection criteria of the substrate. With methyl as the substituent group, the change of Gibbs energy for the deprotonation is only –9.7 kJ/mol, implying that the deprotonation is not complete and there is an equilibrium. Nevertheless, the deprotonation is complete regardless of the electron-withdrawing group on the phenyl ring. It also confirmed that our simplification was appropriate. Based on our calculation results, an aromatic substituent group is required for the deprotonation. Further modifications on the aromatic ring is actually not necessary.

The succinimide moiety was also found to be one of the factors that promote the deprotonation. If the succinimide is replaced by a hydrogen atom, as shown in Scheme 8, the calculated change of free energy now becomes only –17.2 kJ/mol.

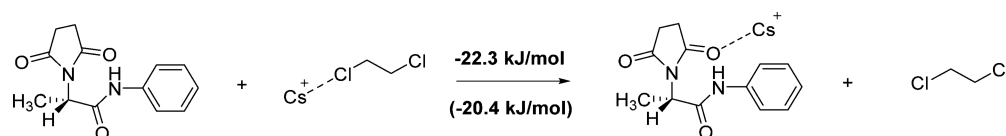
Scheme 8. Enthalpy Change and Gibbs Energy Change for the Deprotonation of the Model Molecule in Which the Succinimide Moiety Is Replaced by H Atom (Gibbs Energy Shown in Parentheses)



Scheme 7. Deprotonation Reaction of Amides with Different Substituent Groups Attached to the N Atom (Gibbs Energy Shown in Parentheses)



Scheme 9. Poor Solvation Ability of DCE (Gibbs Energy Shown in Parentheses)



The selection criteria of amides can be set at this stage based on our calculated data. To activate the precatalyst, a deprotonated amide is needed. An aromatic substituent group and the succinimide moiety are necessary for a complete deprotonation.

1.3. Solvation Effects. Normally, it is difficult for CsF (which is thought to be a weak base) to deprotonate amides since the pK_a of amide is around 17 whereas the pK_a of HF is 3.17. However, in this case, the deprotonation was calculated to be complete. Besides those factors discussed in the former section, the solvent effect plays a very important role for the deprotonation as well. Dichloroethane, which is the solvent used in this reaction, has a very low coordination ability to cesium cation.

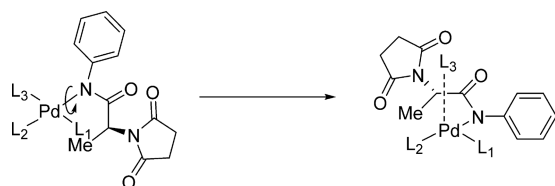
The calculation results shown in Scheme 9 give us a clear picture that the Cs^+ cation would like to be coordinated by the carbonyls of the substrate rather than the DCE molecule. The change of Gibbs energy for the transfer of Cs^+ cation from DCE to the substrate is -20.4 kJ/mol. The carbonyl groups from the substrate, as well as the phenyl ring, bind strongly to the cesium cation.

2. Plausible Pathways for the C–H Activation.

2.1. Prereaction Complex. Having established the mechanism for the initiation step, our concentration now moves to the C–H activation itself. The deprotonated amide replaces one of ligands through a nucleophilic substitution reaction. The ligating atom can be either the N atom or the O atom due to an amide–imidic acid tautomerization. Experiments have revealed that the deprotonated amide tends to bind to Pd via its N atom.³⁹ At the first instance, we concentrate on the reaction pathways involving the N atom as the ligating atom. The pathways with O as the ligating atom will be discussed in the later section.

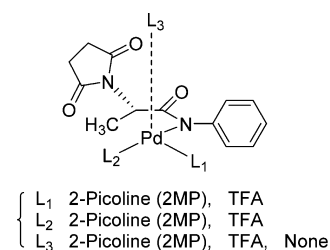
With rotation of the newly formed Pd–N σ -bond, a three-coordinate prereaction complex is therefore generated. The L_3 ligand appearing in the prereaction complex no longer has covalent interaction with the Pd(II) atom, but the electrostatic and dispersion interactions. The prereaction complex demonstrated in Scheme 10 is considered to be the starting point for

Scheme 10. Formation of the Prereaction Complex



all pathways. In the prereaction complex, two equatorial positions are occupied by the amide substrate while the rest are taken by TFA and 2-picoline ligands. It should be noted that only two of the same ligands are allowed to ensure the material input ratio and avoid highly ionic species. Based on this principle, all of the pathways are demonstrated in Table 1.

Table 1. General Structure of the Key Prereaction Intermediates and Plausible Reaction Pathways with Different Ligands



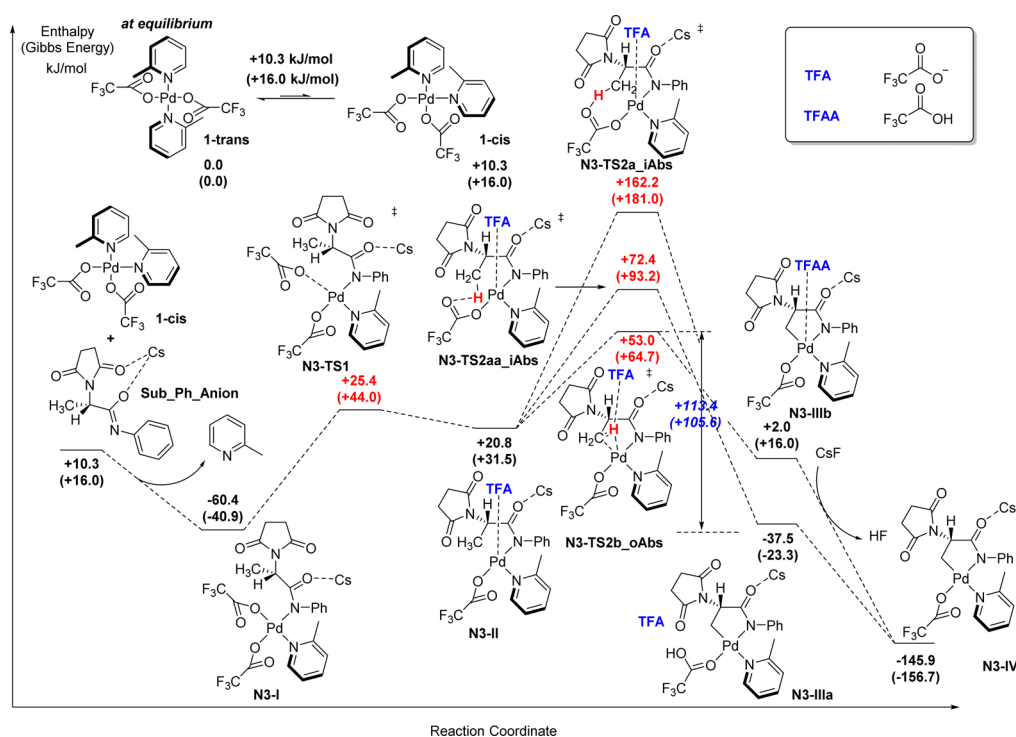
2TFA and 2 2MP are available.

entry	L_1 (equatorial)	L_2 (equatorial)	L_3 (axial, away)
N1	2MP	2MP	TFA
N2	2MP	2MP	None
N3	2MP	TFA	TFA
N4	2MP	TFA	2MP
N5	2MP	TFA	None
N6	TFA	2MP	2MP
N7	TFA	2MP	TFA
N8	TFA	2MP	None
N9	TFA	TFA	2MP
N10	TFA	TFA	None

2.2. Prescreening of the Plausible Pathways. Previous studies suggested that carboxylate ligand is responsible for the H-abstraction,^{40–50} which is known as the concerted metalation deprotonation (CMD) mechanism⁴⁰ or the ambiphilic metal ligand activation (AMLA) mechanism.⁴⁷ The first computational study on such a mechanism was reported in 2001,⁴⁸ followed by two other important articles.^{49,50} In the traditional CMD (or AMLA) mechanism, carboxylate ligand binds to the central metal via one oxygen atom with the other one to abstract proton from the carbon atom. Thus, it can be readily noticed that, among all the pathways listed in Table 1, pathways N2, N6, and N8 are not favorable. It is because that there is no TFA ligand in the vicinity of the methyl group. Therefore, those three pathways can be excluded. Test calculations also confirmed that the energy required for a complete dissociation of the L_3 ligand from the Pd(II) atom is up to 135.2 kJ/mol (see Scheme S11 for details). It is because that the TFA at the L_3 position has strong electrostatic interactions with both the Pd(II) atom and the Cs^+ cation. As mentioned before, since the interaction between L_3 and the rest of the molecule cannot be neglected, pathways N5 and N10 should be omitted as well. Among the remaining five plausible pathways, N1, N3, and N9 start with the precatalyst 1-cis, while N4 and N7 proceed from the predominant 1-trans.

3. Pathways for the Primary C(sp³)–H Activation.

3.1. New Deprotonation Pathway. We started our investigation from pathway 3 since it is the only case in which both L_2 and L_3 positions of the prereaction complex (N3–II) are occupied by TFA ligand. It is necessary to clarify which TFA is responsible for the deprotonation in the minimum energy

Scheme 11. Enthalpy Profile for Pathway N3, in Which Both L₂ and L₃ Positions Are Occupied by TFA Ligands (Gibbs Energy Shown in Parentheses)

pathway (MEP). To our knowledge, the first theoretical investigation on the C–H activation reaction was reported by Sakaki and co-workers in 2001.⁴⁸ Followed by some other contributions,^{49,50} the mechanism that describes the details of the deprotonation and a synchronous C–Metal bond formation was finally named as the concerted metalation deprotonation (CMD) by Fagnou et al.⁴⁰ or the ambiphilic metal ligand activation (AMLA) by Macgregor and co-workers.⁴⁷ The traditional CMD (or AMLA) mechanism is usually adopted to depict those intramolecular deprotonation reactions, in which the base is a carboxylate ligand directly coordinating to the central metal atom. Interestingly, Musaev and co-workers have found that the traditional CMD mechanism does not rationalize the C(sp³)–H activation.³⁸ In that case, the reaction undergoes a Pd(0)–Pd(II)–Pd(0) catalytic cycle without any carboxylate ligand (which facilitates the CMD pathway), and an instant reductive elimination to give out the final product is the driving force for the C–H activation. However, carboxylate ligands, which make the traditional CMD pathway possible, do exist in our case. Thus, it is worth investigating whether the traditional CMD mechanism is still preferred for the C(sp³)–H activation reaction in a Pd(II)–Pd(IV)–Pd(II) catalytic cycle with carboxylic ligands.

As shown in Scheme 11, the reaction starts with the precatalyst 1-cis. The intermediate N3–I is formed after a substitution of 2-picoline (2MP) ligand by the deprotonated amide Sub_Ph_Anion. The TFA (trans to 2MP) is pushed to the axial position with rotation of the Pd–N σ -bond. A vacant site is therefore created in N3–II for the C–H bond to interact with Pd(II) atom. Calculations have revealed that the role of Cs⁺ cation is complicated in this reaction. Not only promoting the deprotonation of amides, the Cs⁺ cation also helps to anchor the TFA ligand which drops from the Pd(II) center via electrostatic interaction. With a TFA staying in the vicinity of

the methyl group (at the L₃ position), an out-of-plane H-abstraction is therefore possible. The word *out-of-plane* is used here since the TFA is above the plane on which the Pd(II) and the rest of ligands stay. A few studies in literature have already suggested that the proton abstraction can be furnished by an acetate ligand from top of the plane.^{51–54} However, those out-of-plane mechanisms discussed in the above articles still followed an intramolecular deprotonation pathway (traditional CMD pathway) in which the acetate is a ligand directly coordinating to the central metal. In our newly proposed out-of-plane pathway, the acetate is no longer a ligand. Thus, our mechanism can be treated as a variant of the traditional CMD pathway. The transition states of our unconventional CMD pathway have been successfully located. Following the traditional CMD pathway, two transition states were also discovered, in which one is called the backside TS and the other one is called the frontside TS, according to Bickelhaupt's work.^{55,56} For the convenience of our discussion, these two transition states which follow the traditional CMD mechanism are labeled as *in-plane* TS.

The single-step Gibbs free energy barrier of the out-of-plane H-abstraction is only 33.2 kJ/mol. The effective Gibbs barriers (based on the energetic span model, suggested by Kozuch et al.^{57–59}) from the most stable intermediate N3–I for the out-of-plane H-abstraction reaction was calculated as only 105.6 kJ/mol. It is clear from Scheme 11 that both in-plane transition states (backside TS and frontside TS) have a higher energy than that of the out-of-plane TS N3-TS2b_oAbs. As shown in Schemes S5 and S6 in the SI, a high barrier applies to other in-plane H-abstractions (pathways N4 and N9). These two pathways are therefore excluded from our consideration.

3.2. Origins of the Out-of-Plane H-Abstraction. Inspection of the corresponding transition states revealed the origins of the out-of-plane H-abstraction. The backside in-plane TS has a

significantly high energy, as indicated in Scheme 11. The Newman projection in Figure 1 shows that four atoms attached

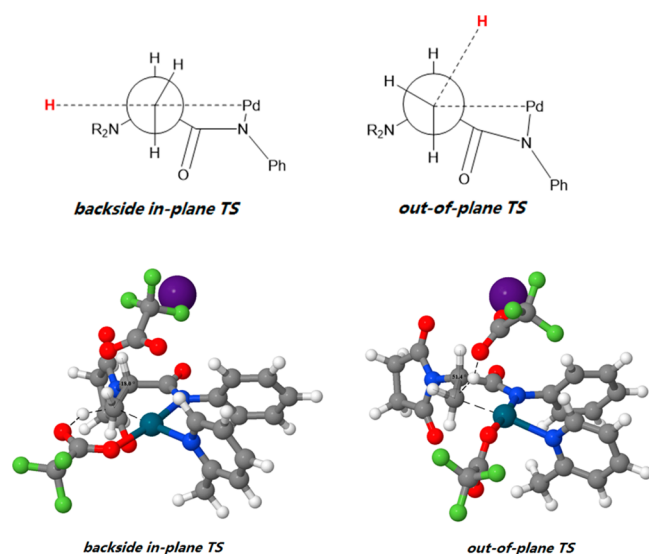


Figure 1. Optimized structures of the transition states of backside in-plane H-abstraction, N3-TS2a-iAbs (left), and out-of-plane H-abstraction, N3-TS2b-oAbs (right).

to the carbon (H, H, H, Pd) are almost perpendicular to each other. Such a severe distortion of the sp^3 -carbon makes the barrier impossible to overcome. The strain on two fused ring in N3-TS2a-iAbs is another reason for the instability. However, compared to N3-TS2a-iAbs, the out-of-plane TS (N3-TS2a-oAbs) shows a favorable gauche C–C conformation. The dihedral H–C–C–H in N3-TS2a-oAbs is in a more comfortable conformation as 51.4° while it is 18.0° in N3-TS2a-iAbs (backside in-plane TS). Furthermore, no ring strain is involved in N3-TS2a-oAbs.

Inspection of N3-TS2aa-iAbs, which is the frontside in-plane TS shown in Figure 2, helps us to understand the reason why it is also high in energy. It is obvious that the moving direction of the proton deviates from the extension line of the original C–H bond. The distortion of the structure makes its Gibbs free energy 28.5 kJ/mol higher than that of the out-of-plane TS (N3-TS3b-oAbs), in which the sp^3 -carbon adopts the most comfortable conformation.

Overall, the $C(sp^3)$ –H activation in this one-pot reaction undergoes an unconventional CMD pathway, in which the base is no longer a ligand directly bound to the Pd(II) atom. Our work reveals that there should be different ways of

deprotonation for the base-assisted C–H activation, depending on the nature of metal and reaction conditions.

3.3. Minimum Energy Pathway. Those pathways involving in-plane H-abstraction have been excluded, as our study on pathway N3 suggested that they have much higher barriers. At this point, pathways N1 and N7 with energetically favored out-of-plane H-abstraction were carefully investigated. The mapped energy profiles for pathways N1 and N7 are shown in Schemes 12 and 13, respectively.

These two pathways are similar to each other, regardless of the different ligands coordinating to the Pd(II) atom. As demonstrated in Scheme 13, pathway N7 starts with the activation reaction of the precatalyst 1-trans. The intermediate N7–I is formed after a substitution of 2-picoline ligand by the deprotonated amide substrate **Sub_Ph_Anion**. An intramolecular rearrangement then takes place to give out the reactive intermediate N7–II in which a TFA moves from the equatorial to the axial position. Then an out-of-plane H-abstraction is conducted as the axial TFA abstracting proton from the methyl group. A simultaneous Pd–C bond formation gives out the product of the C–H activation, labeled as N7–III. The situation is similar for the pathway N1, via N1–I \rightarrow N1–II \rightarrow N1–III (see Scheme 12). Interestingly, calculations indicated that the C–H activation itself does not have a significant driving force. The trifluoroacetic acid (TFAA) formed through the C–H activation is then neutralized by excess CsF (with an initial input of two equivalents). The coupled neutralization reaction is exoergic so that the equilibrium is shifted to the final product, N7–IV or N1–IV.

The effective Gibbs barriers for pathways N1 and N7 are 121.6 and 100.1 kJ/mol, respectively. By considering that the precatalyst 1-trans is more stable and the transformation of 1-trans to 1-cis is kinetically prohibited, the conclusion can be drawn here that pathway N7 is the MEP for this novel $C(sp^3)$ –H activation reaction.

3.4. MEP for the Real Substrate. In the preceding sections, a model system was adopted in our calculations. Since the MEP was found based on our model substrate (see **Computational Details**), it is necessary to apply it to the real substrate (in which the succinimide part is still simplified) in case of an error. The MEP was therefore carefully revisited with the real substrate. Not surprisingly, the effective Gibbs barrier for the real system remains almost unchanged at 105.3 kJ/mol (104.7 kJ/mol for the enthalpy barrier). It confirmed that our mechanism based on the model system is reliable.

3.5. N-Coordination versus O-Coordination. As discussed above, the deprotonated amide can coordinate to the Pd(II) atom via either its N atom or the O atom due to the amide-

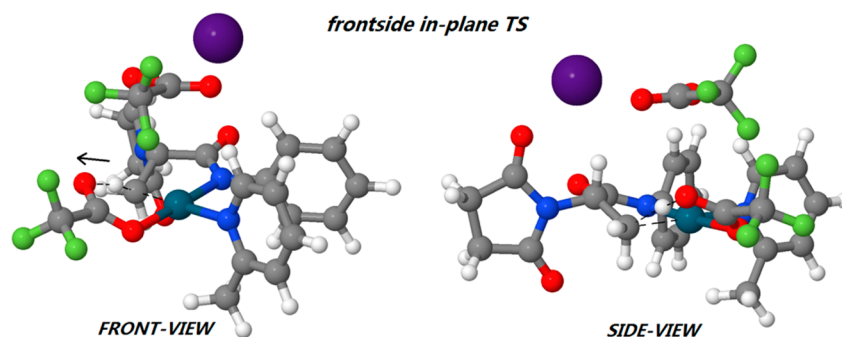
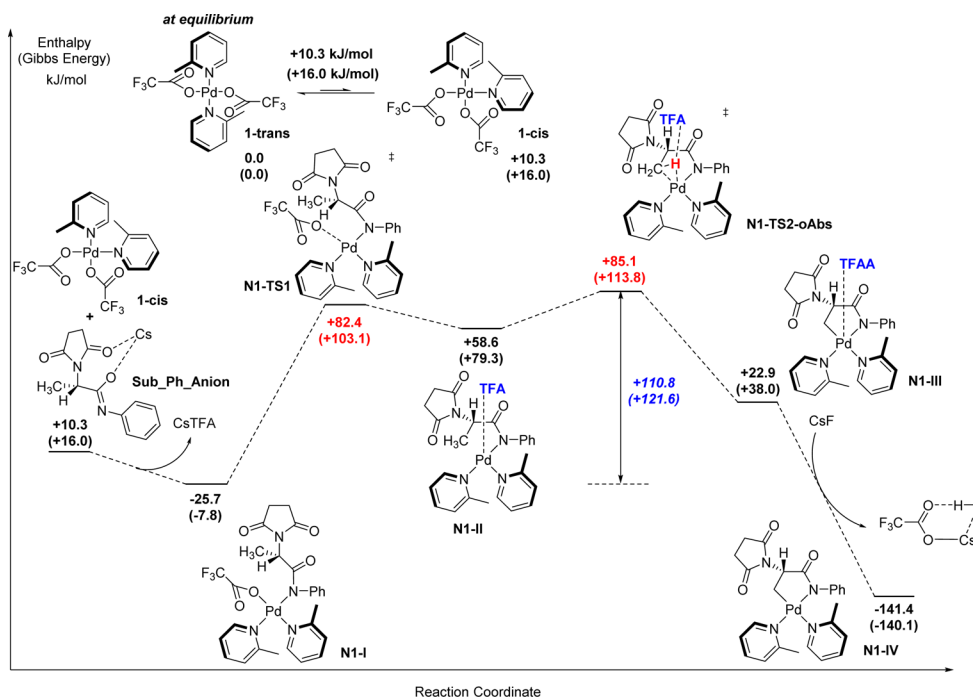
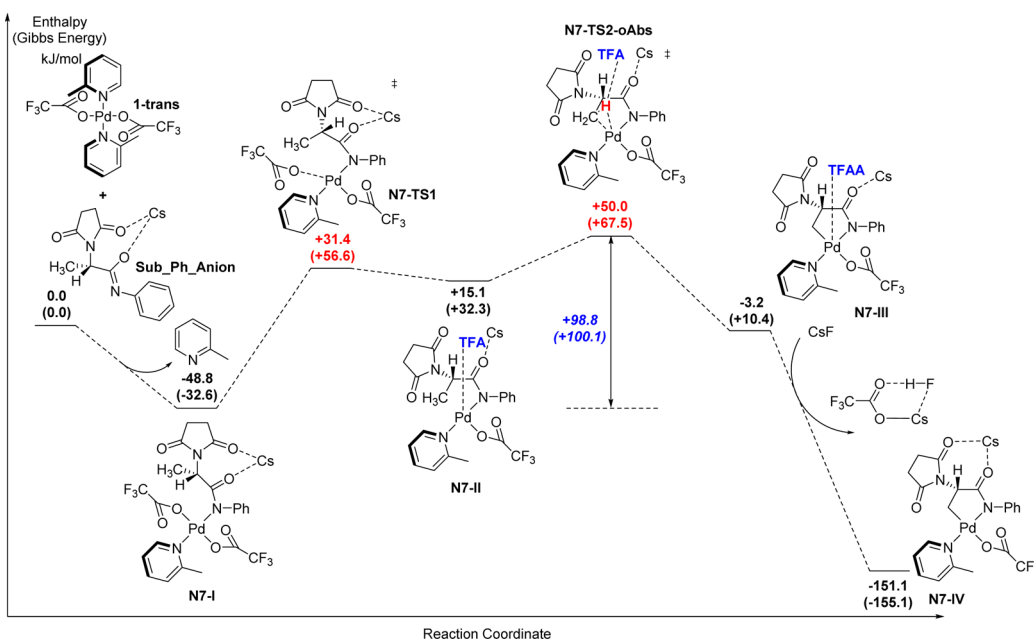


Figure 2. Optimized structures of the transition state of frontside in-plane H-abstraction, N3-TS2aa-iAbs.

Scheme 12. Enthalpy Profile for Pathway N1 with an Out-of-Plane H-Abstraction (Gibbs Energy Shown in Parentheses)



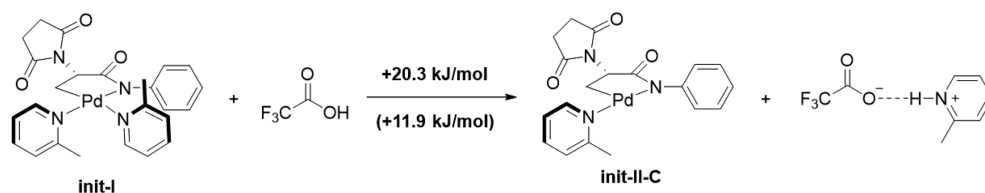
Scheme 13. Enthalpy Profile for Pathway N7 with an Out-of-Plane H-Abstraction (Gibbs Energy Shown in Parentheses)



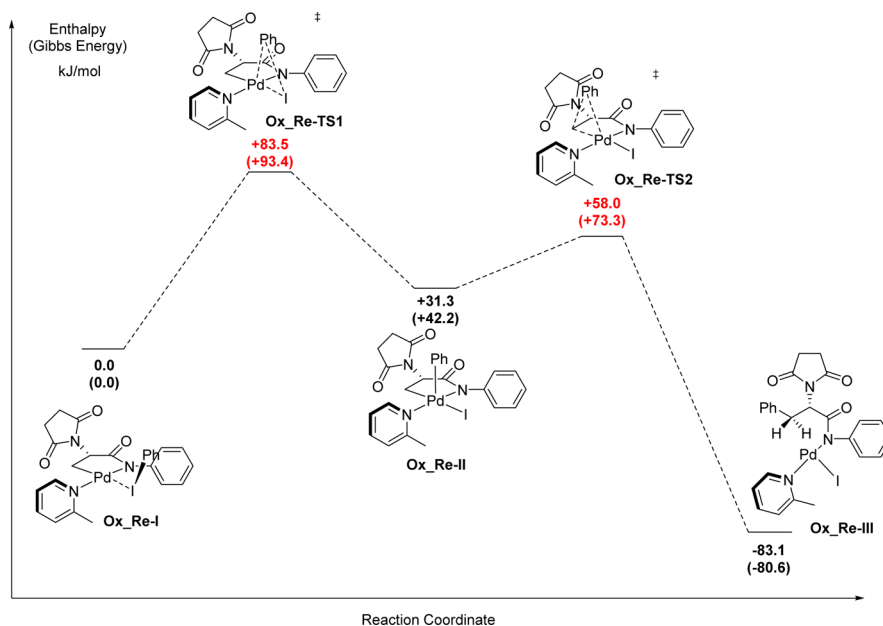
imidic acid tautomerization. As shown in Scheme S7 in the SI, the mechanism of the pathway with O-coordination (pathway O7) is almost as same as pathway N7 in the preceding section. The only difference is that the ligating atom is no longer the N atom but the O atom. However, our calculations suggested an effective Gibbs barrier of 139.2 kJ/mol in this case, which is much higher than that of pathway N7. Inspections of the intermediates and transition states revealed that even the intermediate with a Pd–O bond has a higher energy compared to its isomer with a Pd–N bond. The difference in energy can be rationalized by the HSAB theory⁶⁰ quantitatively. Pd(II) atom, as a soft acid, has a larger affinity to N atom rather than O atom.

4. Arylation Reaction from Intermediate A. **4.1. Initiation of Arylation Reaction.** As part of the one-pot reaction, the next step after the primary C(sp³)–H activation is the arylation reaction. It consists of an oxidative addition of iodobenzene to the Pd(II) atom, followed by a reductive elimination to give the final product. As mentioned above, intermediate A (see Scheme 2), as the product of the primary C(sp³)–H activation, was isolated after quenching and recrystallization. It implied that Cs⁺ cation was removed and some ligand exchanges took place during the termination process of the reaction. In order to make the reaction proceed smoothly, a vacant site has to be created prior to the oxidative addition taking place. Similar to what we indicated before, the

Scheme 14. TFAA Assisted Dissociation of the 2MP Ligand (Gibbs Energy Shown in Parentheses)



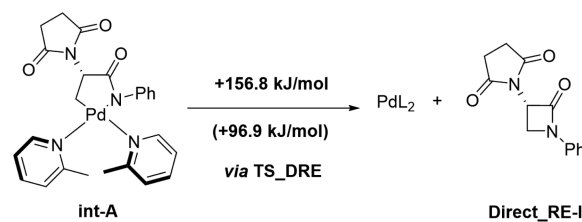
Scheme 15. Enthalpy Profile for the Oxidative Addition and Reductive Elimination



four-coordinate Pd(II) complex **intA** shows a remarkable stability. Our further calculations confirmed that it is difficult to dissociate a 2-picoline (2MP) ligand from the Pd(II) atom, as shown in Scheme S8. The change of enthalpy for losing a ligand is as high as 95.3 kJ/mol. Different from the initiation reaction discussed before, no modification on iodobenzene is possible to make it more nucleophilic. However, as shown in Scheme 14, the dissociation becomes energetically feasible when it is coupled with the neutralization reaction in which trifluoroacetic acid (TFAA) reacts with the leaving 2MP ligand. Our calculations revealed that the *trans*-effect preferentially removes the 2MP ligand trans to the strong σ -donor (the C atom), as shown in Scheme S8. This dissociation of the 2MP ligand generates a three-coordinate intermediate **init-II-C**, which has a vacancy reserved for the incoming iodobenzene.

4.2. Oxidative Addition and Reductive Elimination. The intermediate **init-II-C**, which was generated through a TFAA assisted dissociation reaction, binds to iodobenzene to form a prereaction complex **Ox_Re-I**. As demonstrated in Scheme 15, the oxidative addition has a high Gibbs barrier of 93.4 kJ/mol, due to the steric effect and the change of the oxidation state of the Pd atom. The square pyramidal Pd(IV) intermediate **Ox_Re-II** generated through the oxidative addition then undergoes a barrierless reductive elimination reaction. The phenyl group is thus transferred to the amide substrate to form the intermediate **Ox_Re-III**. This intermediate then goes through ligand exchange to release the arylation product and the Pd(I)(TFA)(L)₂ complex. The latter reacts with ligands in solution to regenerate the catalyst. The arylation product is the starting point for the secondary C(sp³)-H activation reaction.

4.3. Direct Reductive Elimination of int-A. The preceding sections described the Pd(II)-Pd(IV)-Pd(II) reaction schemes. Meanwhile, it is more common to observe a direct reductive elimination for those intermediates bearing a Pd-C bond. As shown in Scheme 16, the direct reductive elimination

Scheme 16. Direct Reductive Elimination of **int-A** (Gibbs Energy Shown in Parentheses)

of **int-A** should result in the formation of an azetidine derivative **Direct_RE-I** and a Pd(0) complex. Nevertheless, our calculations figured out that the reaction is highly endothermic with a change of enthalpy of +156.8 kJ/mol.

More efforts were made to locate the transition state of the direct reductive elimination reaction, which is shown in Figure S1. With the finding of the transition state **TS_DRE**, the Gibbs barrier for the direct reductive elimination was found to be 258.2 kJ/mol (266.9 kJ/mol as the enthalpy barrier). The strong ring strain on the four-membered ring of **TS_DRE** can be used to rationalize such a high barrier. Our calculation results fit the experimental observations that no azetidine was detected in the reaction mixture. By recalling the effective

Scheme 17. Stereoselectivity in the Secondary C–H Activation Step (Gibbs Energy Shown in Parentheses)

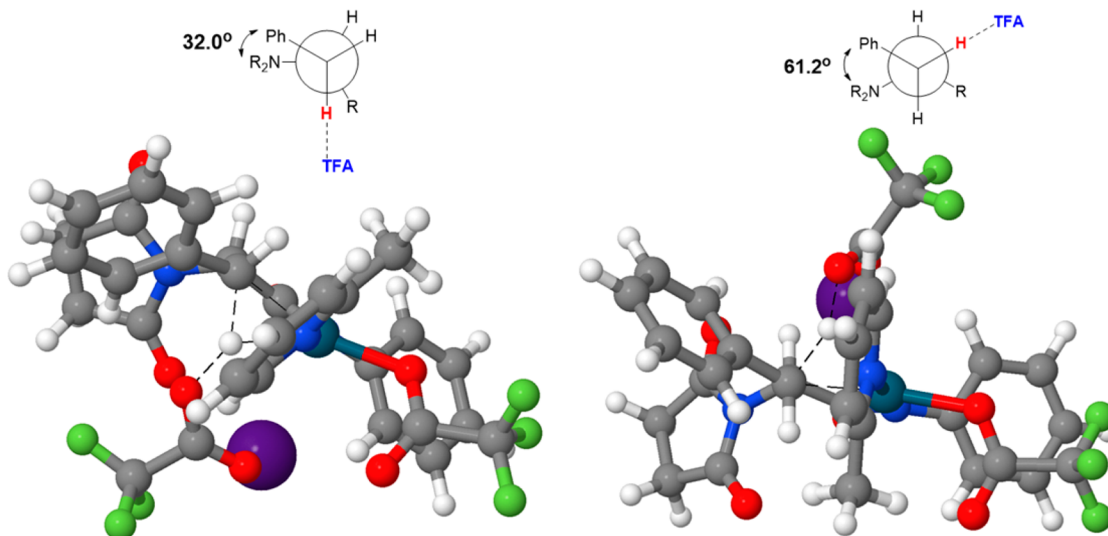
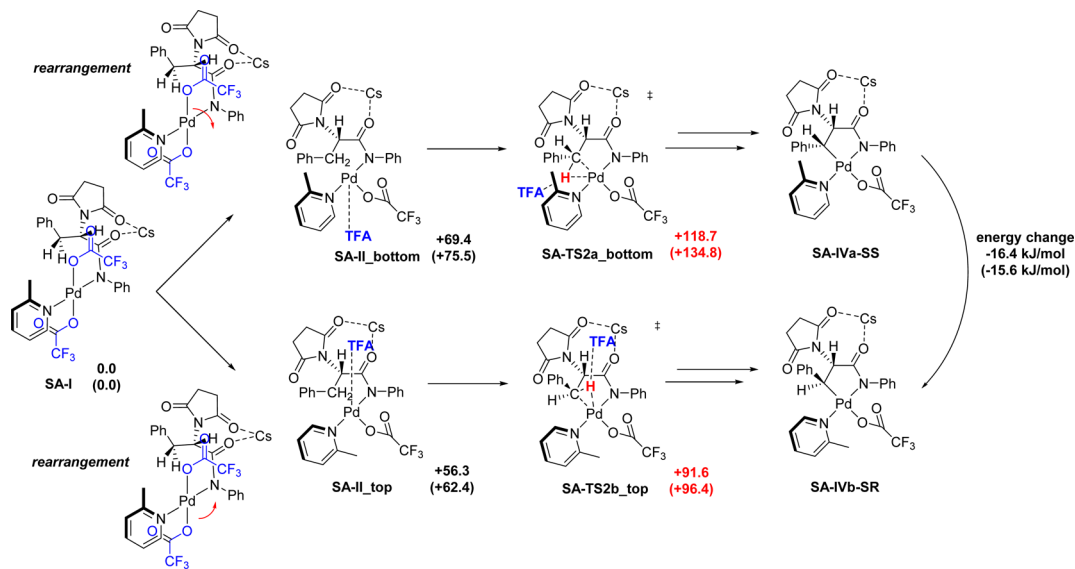


Figure 3. Optimized structures of SA-TS2a_bottom (left, semioverlapped conformation) and SA-TS2b_top (right, gauche conformation).

barrier of the oxidative addition and reductive elimination reactions (as 93.4 kJ/mol), we can understand why intermediate **A**, as the product of a C–H activation reaction, can be isolated successfully.

5. Secondary C(sp³)–H Activation and Origins of Diastereoselectivity. This reaction was employed as a strategy to synthesize unnatural amino acid since the remaining C–H bond could be further functionalized, as shown on the second line of Scheme 1. The reaction on the secondary carbon atom is stereoselective if a different aryl halide is used. The (*S,R*)-product rather than the (*S,S*)-product is always the predominant product. Our studies suggested that the oxidative addition and the following reductive elimination do not affect the chirality of the sp³-carbon atom. Therefore, the absolute configuration of the arylation product is determined at the earliest stage, which is the secondary C(sp³)–H activation step.

As shown in Scheme 17, the product of the first arylation reaction, **SA-I**, was taken as the starting point for the second C–H activation. We note here that one may compare Scheme 17 with Scheme 13, which is the energy profile of the minimum

energy pathway (pathway N7) for the first C–H activation. The only difference is that the plane of coordination square drawn horizontally in Scheme 13 is now drawn vertically for **SA-I** in Scheme 17 to distinguish two TFA ligands with one at the top and the other one at the bottom. The bending of the TFA ligand on the top will push the other to stay below the square plane where the Pd(II) locates, and vice versa. The absolute configuration of the final product shown in Scheme 1 is determined by whether it is the top TFA or the bottom one to abstract proton from the benzyl group (Ph–CH₂–).

As shown in Scheme 17, the compound in (*S,R*) configuration is both the thermodynamically and the kinetically preferred product. The TFA prefers to abstract proton from the top of the plane, keeping the phenyl group on the opposite side with respect to the succinimide moiety. The Gibbs energy difference between two transition states (**SA-TS2b_top** and **SA-TS2a_bottom**) is as large as 38.4 kJ/mol, which clearly indicates the former is preferred. Preference of the structure in which TFA stays above the plane is evident at the prereaction complex **SA-II_top**.

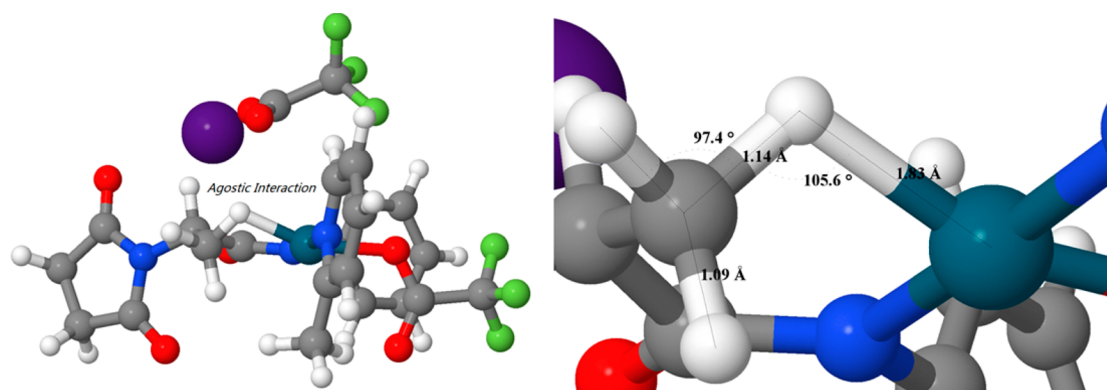


Figure 4. Optimized structure of intermediate N7-II, in which the agostic interaction exists.

Inspections of the optimized structures rationalized the energy difference from a chemistry point of view. The optimized structure of SA-TS2a_bottom in Figure 3 clearly shows that the space below the plane is very crowded, with much short distances and hence a larger steric repulsion between the phenyl group and the succinimide moiety. The dihedral angle of Ph-C-C-N in SA-TS2a_bottom is 32.0° (as a semioverlapped conformation) due to the crowding. However, the dihedral becomes 61.2° as a comfortable gauche conformation in SA-TS2b_top.

Based on the discussions made above, the size of the aryl halide is irrelevant to the diastereoselectivity, since the chirality was determined at the C-H activation step. The applications of this reaction are therefore extended as more kinds of amino acids can be prepared in this way.

Another thing to be mentioned is the role of Cs⁺ cation. As discussed before, the TFA ligand dropping from the Pd(II) atom is fixed through the electrostatic interaction with the Cs⁺ cation, which makes the out-of-plane H-abstraction possible. One may notice that the Cs⁺ cation is always on the same face with respect to the TFA dropping from the Pd(II) center in all of our optimized structures, since they are the most stable conformers.

6. Other Aspects of the C-H Activation. **6.1. Agostic Interaction.** One of the most important findings in our theoretical studies is that we have detected a crucial prereaction intermediate with an agostic bond. The intermediate, labeled as N7-II, is high in energy so that it cannot be detected by any experimental instruments. Agostic interaction is essentially a C-H $\sigma \rightarrow$ metal d donative interaction.^{61,62} The first theoretical study on the agostic interaction was reported in 1984.⁶³ The compounds with agostic interaction are generally unstable, except for some masked three-coordinate Pt(II) complexes which were isolated successfully.^{64–68}

It is clear from the optimized structure of the prereaction intermediate N7-II (Figure 4) that the C-H bond which is about to break extends to 1.14 Å whereas a normal C-H bond is only 1.09 Å long. The C(sp³)-H stretching vibration frequency drops to 2588 cm⁻¹ while the frequency of a normal C(sp³)-H bond is 3070 cm⁻¹. Thus, our calculations clearly suggested that the agostic interaction plays an important role to weaken the C-H bond and facilitate the C-H activation.

Based on the observation that the C-H activation is promoted by the formation of an agostic bond, we have tested the similar system with Pt(II) as the central metal. With Pt(II) as the central metal, the C(sp³)-H bond extends further to 1.18 Å and the C-H stretching vibrational frequency drops to

only 2156 cm⁻¹. The optimized transition state of the C-H activation catalyzed by Pt(II) atom is shown in Figure 5.

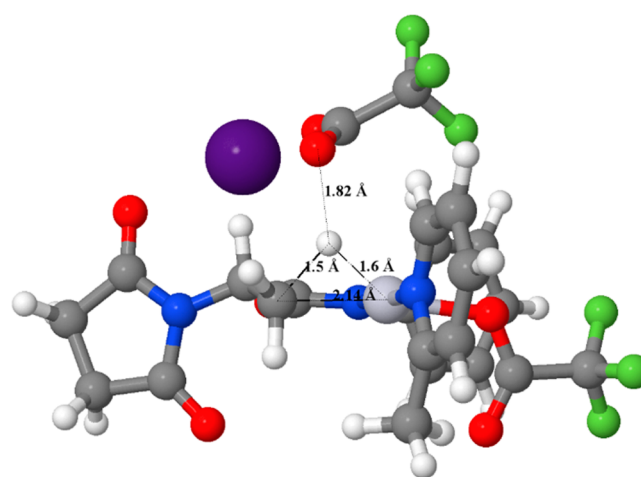


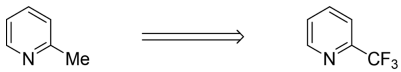
Figure 5. Optimized structure for the TS of C-H activation in which Pt(II) replaces Pd(II).

Inspection of the optimized structure revealed that the proton moves to the Pt(II) atom directly rather than going to the TFA. The overall Gibbs barrier was calculated as low as 74.4 kJ/mol, suggesting that the reaction with Pt(II) catalyst should proceed more smoothly.

6.2. Ligand Effects on Primary C-H Activation. Enhancing the agostic interaction and thus weakening the C-H bond by appropriate choice of ligands is a way to perform more effective primary C(sp³)-H activation. The agostic interaction can be strengthened if the central metal becomes more electrophilic. Electron-deficient ligands, such as 2-nitropyridine and 2-trifluoromethylpyridine, are therefore good candidates for a more effective primary C-H activation. We conducted a preliminary calculation by changing the 2-picoline (2MP) ligand to 2-trifluoromethylpyridine for the C-H activation step based on pathway N7.

It is clearly indicated in Table 2 that the electron-deficient ligand lowers the effective barrier of the primary C(sp³)-H activation. Overall, our calculations offered a systematical strategy to improve the primary C(sp³)-H activation.

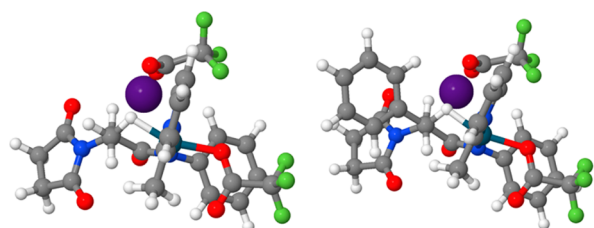
6.3. Ligand Effects on Secondary C(sp³)-H Activation. To rationalize the experimental observation that an electron-rich ligand (quinoline derivatives) boosts the secondary C(sp³)-H activation, we also conducted an atomic partial charge analysis²⁸

Table 2. Effective Barriers (kJ/mol) of the C–H Activation in Pathway N7 with Different Ligands


for the first arylation

ligand	eff. barrier ΔH^\ddagger	eff. barrier ΔG^\ddagger
2-picoline (2MP)	+98.8	+100.1
2-trifluoromethylpyridine	+90.8	+93.0

for N7-II and SA-II_top, which are the prereaction intermediates of the primary and secondary C(sp³)–H activation. As shown in Figure 6, between these two structures there is an obvious umpolung of the carbon atom which is about to connect to the Pd(II) atom during the C–H activation.

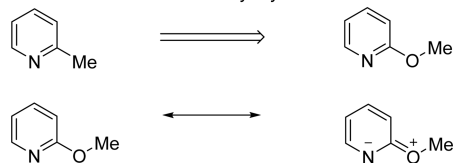


APT Charges C : -0.039 Pd : +1.153 APT Charges C : +0.146 Pd : +1.187

Figure 6. APT partial charge analysis for N7-II (left) and SA-II_top (right), pre-reaction complexes of the primary and secondary C(sp³)–H activation.

It is clear in Figure 6 that the APT charge on the carbon atom changes the sign from -0.039 (CH₃) to $+0.146$ (CH₂Ph). In general, a phenyl group can donate electron density to a conjugated system. Nevertheless, if a phenyl group is directly connected to an alkyl group, it becomes an electron-withdrawing group due to a higher electronegativity of the carbon atom in sp² hybridization form. Therefore, the Pd(II) atom needs to be nucleophilic to accept the carbon, due to the umpolung discussed above. It is opposite to what we discussed in the primary C(sp³)–H activation reaction that an electrophilic Pd(II) atom promotes the C–H activation. Thus, at the secondary C(sp³)–H activation step, efforts should be made to increase the nucleophilicity of the Pd(II) atom. An electron-rich ligand, rather than an electron-poor ligand, should be employed in this case.

The calculation results shown in Table 3 revealed that the effective Gibbs barrier for the secondary C(sp³)–H activation,

Table 3. Effective Barriers of the Secondary C–H Activation with Different Ligands


for the secondary arylation

ligand	eff. barrier ΔH^\ddagger	eff. barrier ΔG^\ddagger
2-picoline (2MP)	+91.6	+96.4
2-methoxypyridine	+85.5	+92.7

in which an electron-rich ligand (2-methoxypyridine) is used, is 3.7 kJ/mol lower than that of the reaction with a 2-picoline (2MP) ligand. The reaction conditions for the secondary C(sp³)–H activation and the subsequent arylation with quinolone ligand became milder accordingly, as proven by the experiments (see Scheme 2 for details).

6.4. Further Application. According to our calculations, this reaction represents a new strategy to facilitate C(sp³)–H activation. Thus, the applicability of this reaction may be not restricted within the synthesis of amino acids. Many cyclic amines are treated as the important precursors in pharmaceutical industry due to their bioactivity.⁶⁹ Many contributions have been made to functionalize the α -position of the cyclic amines.⁷⁰

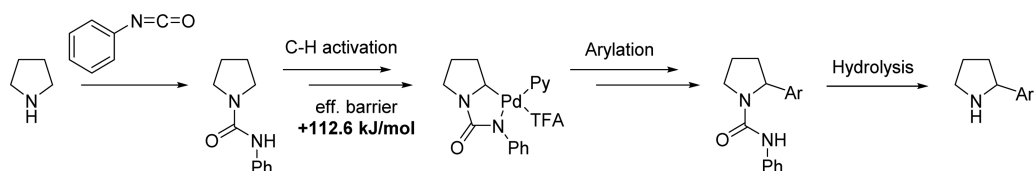
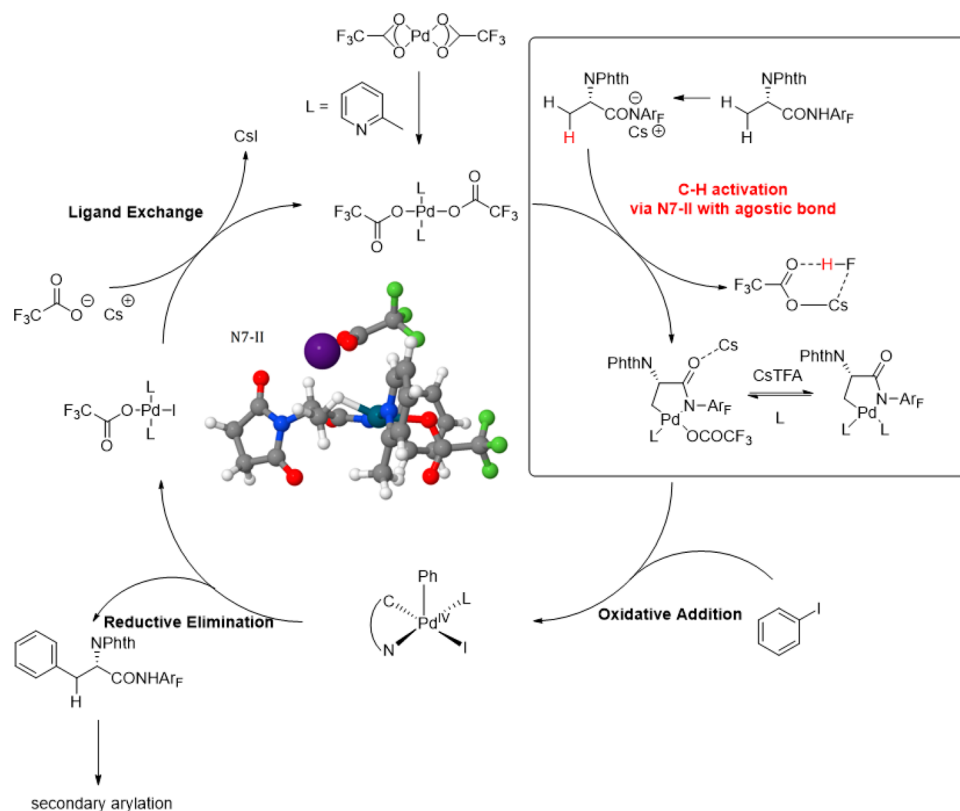
Having established the detailed mechanism for this C–H activation via DFT calculations, we envisaged that this reaction might be employed to the C(sp³)–H bond of cyclic compounds as well. Thus, we performed further calculations to test our prediction on the α -functionalization of cyclic amines. Tetrahydropyrrole was chosen as the model molecule as the cyclic amine. As what was found that the amide moiety is crucial to the C–H activation, some modifications are necessary prior to the C(sp³)–H activation reaction. The simplified synthetic pathway is shown in Scheme 18 in which the C–H activation is the most important step.

Our calculation results indicated that the effective Gibbs barrier for the C–H activation is 112.6 kJ/mol, which implies that this reaction is possible from our theoretical point of view.

CONCLUSIONS

In this article, various aspects of a novel C(sp³)–H activation and arylation reaction were discussed. Attention was mainly focused on the C–H activation step. A four-coordinate Pd(II) complex **1-trans** was formed accordingly with the presence of 2-picoline ligand. A deprotonated amide is necessary to activate the inert precatalyst **1-trans**. The deprotonation is achieved based on several factors, including the structure of the amide, the solvent effect and the cesium effect. Different from what is described by the traditional CMD (or AMLA as suggested by Macgregor et al.) mechanism, the H-abstraction in this reaction is conducted by an out-of-plane TFA which has no covalent interaction with the Pd(II) atom. Inspection of the corresponding transition states shows that the conformation of the sp³-C atom is distorted in the TS which follows the traditional CMD mechanism. Our work indicates that the traditional CMD mechanism, in which the base is a ligand directly coordinating to the central metal, is not applicable to this C(sp³)–H activation. Pathway N7 was found as the MEP for the primary C(sp³)–H activation. The product of the primary C(sp³)–H activation (intermediate **A**) is reactivated by trifluoroacetic acid for the subsequent oxidative addition and reductive elimination. Based on the calculation discussed so far, a reasonable mechanism is proposed and shown in Scheme 19.

The origin of the stereoselectivity in the secondary C(sp³)–H bond functionalization was found to be the energy gap between two transition states at the secondary C(sp³)–H activation step. The steric repulsion between the phenyl group and the succinimide moiety is crucial to the selectivity. The size of the aryl halide for the C–H bond functionalization is irrelevant to the selectivity, since the stereochemistry of the final product is determined at the C–H activation step rather than the oxidative addition step. More kinds of amino acids may be prepared in this way.

Scheme 18. Arylation on the α -Position of TetrahydropyrroleScheme 19. Proposed Mechanism of the Primary $C(sp^3)$ -H Activation and Arylation Reactions

Our calculations suggested that the agostic interaction is essential in weakening the C–H bond based on the inspection of the prereaction complex. Pt(II) was found to have a stronger agostic interaction with the C–H bond, which promotes the C–H activation. Some other aspects, including the ligand effect and the further application of this reaction, were also mentioned in this article.

■ ASSOCIATED CONTENT

📄 Supporting Information

The Supporting Information is available free of charge on the ACS Publications website at DOI: 10.1021/cs501626n.

Energy profiles, reactions schemes, and structures, as well as Cartesian coordinates and absolute energies of all optimized structures (PDF)

■ AUTHOR INFORMATION

Corresponding Author

*E-mail: morokuma@fukui.kyoto-u.ac.jp.

Notes

The authors declare no competing financial interest.

■ ACKNOWLEDGMENTS

This work was partly supported by Grants-in-Aid from MEXT for Scientific Research (A) (No. 24245005 and 15H02158) and for Innovative Areas (stimuli-responsive chemical species, No. 25109525 and 15H00938) at Kyoto University. The computer resources at the Academic Center for Computing and Media Studies (ACCMS) at Kyoto University and Research Center of Computer Science (RCCS) at the Institute for Molecular Science are also acknowledged.

■ REFERENCES

- (1) Yin, L.; Liebscher, J. *Chem. Rev.* **2007**, *107*, 133–173.
- (2) Heck, R. F.; Nolley, J. P. *J. Org. Chem.* **1972**, *37*, 2320–2322.
- (3) Miyaura, N.; Yamada, K.; Suzuki, A. *Tetrahedron Lett.* **1979**, *20*, 3437–3440.
- (4) King, A. O.; Okukado, N.; Negishi, E. *J. Chem. Soc., Chem. Commun.* **1977**, *19*, 683–684.
- (5) Stille, J. K. *Angew. Chem., Int. Ed. Engl.* **1986**, *25*, 508–524.
- (6) Sonogashira, K.; Tohda, Y.; Hagihara, N. *Tetrahedron Lett.* **1975**, *16*, 4467–4470.
- (7) Huang, J.; Macdonald, S. J. F.; Harrity, J. P. A. *Chem. Commun.* **2010**, *46*, 8770–8772.
- (8) Chen, X.; Engle, K. M.; Wang, D.; Yu, J. *Angew. Chem., Int. Ed.* **2009**, *48*, 5094–5115.

- (9) Li, G.; Leow, D.; Wan, L.; Yu, J. *Angew. Chem., Int. Ed.* **2013**, *52*, 1245–1247.
- (10) Tang, R.; Li, G.; Yu, J. *Nature* **2014**, *507*, 215–220.
- (11) He, J.; Li, S.; Deng, Y.; Fu, H.; Laforteza, B. N.; Spangler, J. E.; Homs, A.; Yu, J. *Science* **2014**, *343*, 1216–1220.
- (12) (a) Becke, A. D. *Phys. Rev. A: At., Mol., Opt. Phys.* **1988**, *38*, 3098–3100. (b) Becke, A. D. *J. Chem. Phys.* **1993**, *98*, 1372–1377.
- (13) Lee, C.; Yang, W.; Parr, R. G. *Phys. Rev. B: Condens. Matter Mater. Phys.* **1988**, *37*, 785–789.
- (14) Grimme, S.; Anthony, J.; Ehrlich, S.; Krieg, H. *J. Chem. Phys.* **2010**, *132*, 154104–1.
- (15) Frisch, M. J.; Trucks, G. W.; Schlegel, H. B.; Scuseria, G. E.; Robb, M. A.; Cheeseman, J. R.; Scalmani, G.; Barone, V.; Mennucci, B.; Petersson, G. A.; Nakatsuji, H.; Caricato, M.; Li, X.; Hratchian, H. P.; Izmaylov, A. F.; Bloino, J.; Zheng, G.; Sonnenberg, J. L.; Hada, M.; Ehara, M.; Toyota, K.; Fukuda, R.; Hasegawa, J.; Ishida, M.; Nakajima, T.; Honda, Y.; Kitao, O.; Nakai, H.; Vreven, T.; Montgomery, J. A., Jr.; Peralta, J. E.; Ogliaro, F.; Bearpark, M.; Heyd, J. J.; Brothers, E.; Kudin, K. N.; Staroverov, V. N.; Kobayashi, R.; Normand, J.; Raghavachari, K.; Rendell, A.; Burant, J. C.; Iyengar, S. S.; Tomasi, J.; Cossi, M.; Rega, N.; Millam, M. J.; Klene, M.; Knox, J. E.; Cross, J. B.; Bakken, V.; Adamo, C.; Jaramillo, J.; Gomperts, R.; Stratmann, R. E.; Yazyev, O.; Austin, A. J.; Cammi, R.; Pomelli, C.; Ochterski, J. W.; Martin, R. L.; Morokuma, K.; Zakrzewski, V. G.; Voth, G. A.; Salvador, P.; Dannenberg, J. J.; Dapprich, S.; Daniels, A. D.; Farkas, Ö.; Foresman, J. B.; Ortiz, J. V.; Cioslowski, J.; Fox, D. J. *Gaussian 09, Revision D.01*; Gaussian, Inc.: Wallingford CT, 2009.
- (16) Krishnan, R.; Binkley, J. S.; Seeger, R.; Pople, J. A. *J. Chem. Phys.* **1980**, *72*, 650–654.
- (17) Dolg, M. *Theor. Comput. Chem.* **2002**, *11*, 793–862.
- (18) Hollwarth, A.; Böhme, M.; Dapprich, S.; Ehlers, A. W.; Gobbi, A.; Jonas, V.; Köhler, K. F.; Stegmann, R.; Veldkamp, A.; Frenking, G. *Chem. Phys. Lett.* **1993**, *208*, 237–240.
- (19) Ehlers, A. W.; Böhme, M.; Dapprich, S.; Gobbi, A.; Höllwarth, A.; Jonas, V.; Köhler, K. F.; Stegmann, R.; Veldkamp, A.; Frenking, G. *Chem. Phys. Lett.* **1993**, *208*, 111–114.
- (20) Peng, C.; Schlegel, H. B. *Isr. J. Chem.* **1993**, *33*, 449–454.
- (21) Peng, C.; Ayala, P. Y.; Schlegel, H. B.; Frisch, M. J. *J. Comput. Chem.* **1996**, *17*, 49–56.
- (22) Schlegel, H. B. *J. Comput. Chem.* **1982**, *3*, 214–218.
- (23) Cancès, M. T.; Mennucci, B.; Tomasi, J. *J. Chem. Phys.* **1997**, *107*, 3032–3041.
- (24) Mennucci, B.; Tomasi, J. *J. Chem. Phys.* **1997**, *106*, 5151–5158.
- (25) Cossi, M.; Barone, V.; Mennucci, B.; Tomasi, J. *Chem. Phys. Lett.* **1998**, *286*, 253–260.
- (26) Cossi, M.; Scalmani, G.; Rega, N.; Barone, V. *J. Chem. Phys.* **2002**, *117*, 43–54.
- (27) Fukui, K. *Acc. Chem. Res.* **1981**, *14*, 363–368.
- (28) Cioslowski, J. *J. Am. Chem. Soc.* **1989**, *111*, 8333–8336.
- (29) Strajbl, M.; Sham, Y. Y.; Villa, J.; Chu, Z. T.; Warshel, A. *J. Phys. Chem. B* **2000**, *104*, 4578–4584.
- (30) Mammen, M.; Shakhnovich, E. I.; Deutch, J. M.; Whiteslides, G. M. *J. Org. Chem.* **1998**, *63*, 3821–3830.
- (31) Ribeiro, R. F.; Marenich, A. V.; Cramer, C. J.; Truhlar, D. G. *J. Phys. Chem. B* **2011**, *115*, 14556–14562.
- (32) Suárez, E.; Díaz, N.; Suárez, D. *J. Chem. Theory Comput.* **2011**, *7*, 2638–2653.
- (33) Cao, Y.; Osuna, S.; Liang, Y.; Haddon, R. C.; Houk, K. N. *J. Am. Chem. Soc.* **2013**, *135*, 17643–17649.
- (34) Crépin, D. F. P.; Harrity, J. P. A.; Jiang, J.; Meijer, A. J. H. M.; Nassoy, A. M. A.; Raubo, P. *J. Am. Chem. Soc.* **2014**, *136*, 8642–8653.
- (35) Plata, R. E.; Singleton, D. A. *J. Am. Chem. Soc.* **2015**, *137*, 3811–3826.
- (36) Sedov, I. A.; Solomonov, B. N. *J. Chem. Eng. Data* **2011**, *56*, 1438–1442.
- (37) Trend, R. M.; Ramtohl, Y. K.; Stoltz, B. M. *J. Am. Chem. Soc.* **2005**, *127*, 17778–17788.
- (38) Figg, T. M.; Wasa, M.; Yu, J.; Musaev, D. G. *J. Am. Chem. Soc.* **2013**, *135*, 14206–14214.
- (39) Menabue, L.; Saladini, M.; Sola, M. *Inorg. Chem.* **1990**, *29*, 1293–1295.
- (40) Gorelsky, S. I.; Lapointe, D.; Fagnou, K. *J. Am. Chem. Soc.* **2008**, *130*, 10848–10849.
- (41) Lyons, T. W.; Sanford, M. S. *Chem. Rev.* **2010**, *110*, 1147–1169.
- (42) Musaev, D. G.; Kaledin, A.; Shi, B.; Yu, J. *J. Am. Chem. Soc.* **2012**, *134*, 1690–1698.
- (43) Li, W.; Sun, P. *J. Org. Chem.* **2012**, *77*, 8362–8366.
- (44) Zhang, L.; Fang, D. *J. Org. Chem.* **2013**, *78*, 2405–2412.
- (45) Munz, D.; Meyer, D.; Strassner, T. *Organometallics* **2013**, *32*, 3469.
- (46) Yang, Y.; Cheng, G.; Liu, P.; Leow, D.; Sun, T.; Chen, P.; Zhang, X.; Yu, J.; Wu, Y.; Houk, K. N. *J. Am. Chem. Soc.* **2014**, *136*, 344–355.
- (47) Boutadla, Y.; Davies, D. L.; Macgregor, S. A.; Poblador-Bahamonde, A. I. *Dalton Trans.* **2009**, 5820–5831.
- (48) Biswas, B.; Sugimoto, M.; Sakaki, S. *Organometallics* **2000**, *19*, 3895–3908.
- (49) Davies, D. L.; Donald, S. M. A.; Macgregor, S. A. *J. Am. Chem. Soc.* **2005**, *127*, 13754–13755.
- (50) Garcia-Cuadrado, D.; Braga, A. A. C.; Maseras, F.; Echavarren, A. M. *J. Am. Chem. Soc.* **2006**, *128*, 1066–1067.
- (51) Chaumontet, M.; Piccardi, R.; Audic, N.; Hitce, J.; Peglion, J.; Clot, E.; Baudoin, O. *J. Am. Chem. Soc.* **2008**, *130*, 15157–15166.
- (52) Kefalidis, C. E.; Baudoin, O.; Clot, E. *Dalton Trans.* **2010**, *39*, 10528–10535.
- (53) Rousseaux, S.; Davi, M.; Sofack-Kreutzer, J.; Pierre, C.; Kefalidis, C. E.; Clot, E.; Fagnou, K.; Baudoin, O. *J. Am. Chem. Soc.* **2010**, *132*, 10706–10716.
- (54) Kefalidis, C. E.; Davi, M.; Holstein, P. M.; Clot, E.; Baudoin, O. *J. Org. Chem.* **2014**, *79*, 11903–11910.
- (55) Diefenbach, A.; Bickelhaupt, F. M. *J. Phys. Chem. A* **2004**, *108*, 8460–8466.
- (56) Diefenbach, A.; Theodoor de Jong, G.; Bickelhaupt, F. M. *J. Chem. Theory Comput.* **2005**, *1*, 286–298.
- (57) Kozuch, S.; Shaik, S. *Acc. Chem. Res.* **2011**, *44*, 101–110.
- (58) Kozuch, S.; Martin, J. M. L. *ChemPhysChem* **2011**, *12*, 1413–1418.
- (59) Kozuch, S. *Wiley Interdiscip. Rev.: Comput. Mol. Sci.* **2012**, *2*, 795–815.
- (60) Pearson, R. G. *J. Am. Chem. Soc.* **1963**, *85*, 3533–3539.
- (61) Brookhart, M.; Green, M. L. H. *J. Organomet. Chem.* **1983**, *250*, 395–408.
- (62) Brookhart, M.; Green, M. L. H.; Parkin, G. *Proc. Natl. Acad. Sci. U. S. A.* **2007**, *104*, 6908–6914.
- (63) Koga, N.; Obara, S.; Morokuma, K. *J. Am. Chem. Soc.* **1984**, *106*, 4625–4626.
- (64) Carr, N.; Dunne, B. J.; Orpen, A. G.; Spencer, J. L. *J. Chem. Soc., Chem. Commun.* **1988**, 926–928.
- (65) Carr, N.; Dunne, B. J.; Mole, L.; Orpen, A. G.; Spencer, J. L. *J. Chem. Soc., Dalton Trans.* **1991**, 863–871.
- (66) Ingleson, M.; Mahon, M. F.; Weller, A. S. *Chem. Commun.* **2004**, 2398–2399.
- (67) Crosby, S. H.; Clarkson, G. J.; Rourke, J. P. *J. Am. Chem. Soc.* **2009**, *131*, 14142–14143.
- (68) Ortuño, M. A.; Conejero, S.; Lledós, A. *Beilstein J. Org. Chem.* **2013**, *9*, 1352–1382.
- (69) Roughley, S. D.; Jordan, A. M. *J. Med. Chem.* **2011**, *54*, 3451–3479.
- (70) Mitchell, E. A.; Peschiulli, A.; Lefevre, N.; Meerpoel, L.; Maes, B. U. W. *Chem. - Eur. J.* **2012**, *18*, 10092–10142.